BEHAVIOR OF CONCRETE WALLS REINFORCED BY ULTRA HIGH-STRENGTH REBARS UNDER DYNAMIC AND STATIC LOADING

C. Wei [(1)], Y. Sun [(2)], T. Takeuchi [(3)], T. Fujitani [(4)]

[(1)] *Ph.D. Student, Graduate School of Engineering, Kobe University, weichengjin1994@gmail.com*
[(2)] *Professor, Graduate School of Engineering, Kobe University, sun@person.kobe-u.ac.jp*
[(3)] *Assistant Professor, Graduate School of Engineering, Kobe University, takeuchi_t@person.kobe-u.ac.jp*
[(4)] *HASEKO Corporation, fujitani3217@gmail.com*

Abstract

A simple and effective reinforcing method is proposed in this paper to make drift-hardening concrete walls with reduced residual deformation and crack width. In the proposed method, the ultra-high yield strength and low bond strength bars (referred to as SBPDN rebar) are utilized as the longitudinal reinforcing bars placed in the edge zone of concrete wall panel in lieu of general normal-strength (NS) deformed rebars.

To verify seismic behavior of the concrete walls reinforced by SBPDN rebars, three rectangular concrete walls were fabricated and tested under pseudo-dynamic loading and/or statically cyclic loading while subjected to a constant compression. All test walls were 900mm and 150mm in depth and width, respectively. The distance from the action line of the lateral loading, pseudo-dynamic and static, to the base of wall was 2025mm to give a shear span ratio of 2.25. The experimental variables were the loading type (dynamic and static) and the configuration of SBPDN rebars placed in the boundary element (parallel placement and inverted V-shaped placement). NS D10 rebars with spacing of 166mm and D6 rebars with spacing of 65mm were adopted as the distributed longitudinal and transverse reinforcement in the wall panel of each specimen, respectively, to give a steel ratio of about 0.65%. Ready-mixed concrete with a designed compressive strength of 40MPa was used to make the walls. The primary tensile rebars in the boundary element consisted of four SBPDN rebars with a specific yield strength of 1275MPa and the tensile steel ratio of SBPDN rebars was about 0.37%. In two walls the SBPDN rebars were placed within edge zones parallel to the axis of wall, while in the other the SBPDN rebars were placed in an inverted V-shape within the wall panel. Of three walls, two were tested under reversed cyclic lateral loading and the other was subjected to pseudo-dynamic loading to investigate the effect of the loading rate on the seismic properties of drift-hardening concrete walls.

Test results shown that the use of SBPDN rebars, regardless of their configuration, could keep the lateral resistance of concrete walls until the drift level of 3.0% without degradation and reduce the residual drift ratio significantly as compared with conventional ductile concrete walls. Test results also indicated that the residual drift of the wall under pseudo-dynamic loading was much less than those of the walls under static cyclic loading. In addition, it was verified that the placement of SBPDN rebars in an inverted V-shape was effective to enhance the shear capacity and prevent the walls from shear failure at larger drift level than 3.0%.

Parallel to experimental work, an analytical method was presented to take account of effect of slippage of the SBPDN rebars and evaluate the cyclic behavior of the proposed drift-hardening concrete walls. Very satisfactory agreement was observed between the experimental hysteresis loops and the theoretical results, which implies the reliability and accuracy of the proposed analytical method.

Keywords: Ultra high-strength rebar, concrete wall, pseudo-dynamic loading, static loading, residual deformation

1. Introduction

Concrete wall with rectangular cross sections is increasingly applied to optimize economy and design among the world. Whereas, the "barbell-shaped" concrete walls consisting of a thin wall web and one or two columns at the web wall edges has been primarily used in Japan since the 1970s. And nowadays, the revised AIJ Standard for Structural Calculation of Reinforced Concrete Buildings in 2010 [1] permits the use of concrete walls with rectangular cross section. A concrete wall with rectangular cross section (referred to as rectangular wall hereafter) has the advantage of increasing the freedom in building design, but as a structural element of horizontal resistance, it must have high ductility because it has less stiffness and strength than a wall with pillars at both ends. For this reason, it is common to arrange longitudinal reinforcing bars intensively at both ends of the wall (referred to as tensile rebars hereafter) as boundary elements in a rectangular wall to improve the stiffness and the bending strength of the wall.

Fujitani et al. [2] used ultra-high-strength reinforcing bars (referred to as SBPDN rebars hereafter) as tensile rebars in a rectangular wall and arranged them as boundary elements parallel to the axis of wall to develop a drift-hardening wall, which presented great drift-hardening capability and reduced residual deformation and crack width. Wei et al. [3] arranged the tensile rebars in an inverted V-shape placement in a cantilever concrete wall to effectively increase the shear strength of the test walls, and the walls also exhibited high deformation performance than the paralleled-reinforced wall.

The purpose of this study is to identify the efficiency that the residual deformation of a concrete wall can be suppressed through the application of SBPDN bars as tensile rebars in the case of dynamic loading as well as static loading. In this study, the SBPDN bars in two walls were placed as parallel placement, while in the other the SBPDN rebars were placed in an inverted V-shaped placement. Of three walls, one of the paralleled-reinforced walls was subjected to pseudo-dynamic loading to investigate the effect of the loading rate on the seismic properties of drift-hardening concrete walls and the other two were tested under reversed cyclic lateral loading for comparison.

2. Experimental program

2.1 Details of test walls

To verify seismic behavior of the concrete walls reinforced by SBPDN rebars, three rectangular concrete walls were fabricated and tested under pseudo-dynamic loading and/or statically cyclic loading while subjected to a constant compression. Fig.1 shows the dimensions and reinforcement details of the three one-second scale cantilever walls, while Table 1 lists the primary experimental parameters along with the main test results. The mechanical properties of the used steels are summarized in Table 2.

Table 1 – Details and estimated ultimate capacities of the test walls

Notation	f_c (Mpa)	a/D	n	Transverse rebars		Longitudinal rebars		Tensile rebars in the boundary element		$V_{fu,NewRC}$ (kN)	$_{exp}Q$ (kN)	$_{exp}Q/V_{fu,NewRC}$
				Type	p_{wh} (%)	Type	p_{wv} (%)	Type	p_t (%)			
WCPS	40.1	2.25	0.075	D6	0.65	D10	0.63	U12.6	0.37	362.6	365.0	1.01
WCPD	42.9	2.25	0.075	D6	0.65	D10	0.63	U12.6	0.37	369.2	367.7	1.00
WCTS	43.7	2.25	0.075	D6	0.65	D10	0.63	U12.6	0.37	347.5	340.1	0.98

Note: f_c -concrete cylinder strength; a/D -shear span ratio; n-axial load ratio; p_{wv} -the steel ratio of longitudinal reinforcement bars; p_{wh} -the steel ratio of transverse reinforcement bars; p_t -the steel ratio of tensile rebars; $V_{fu,NewRC}$ -the ultimate flexural capacity by NewRC block; $_{exp}Q$- the maximum of experimental values

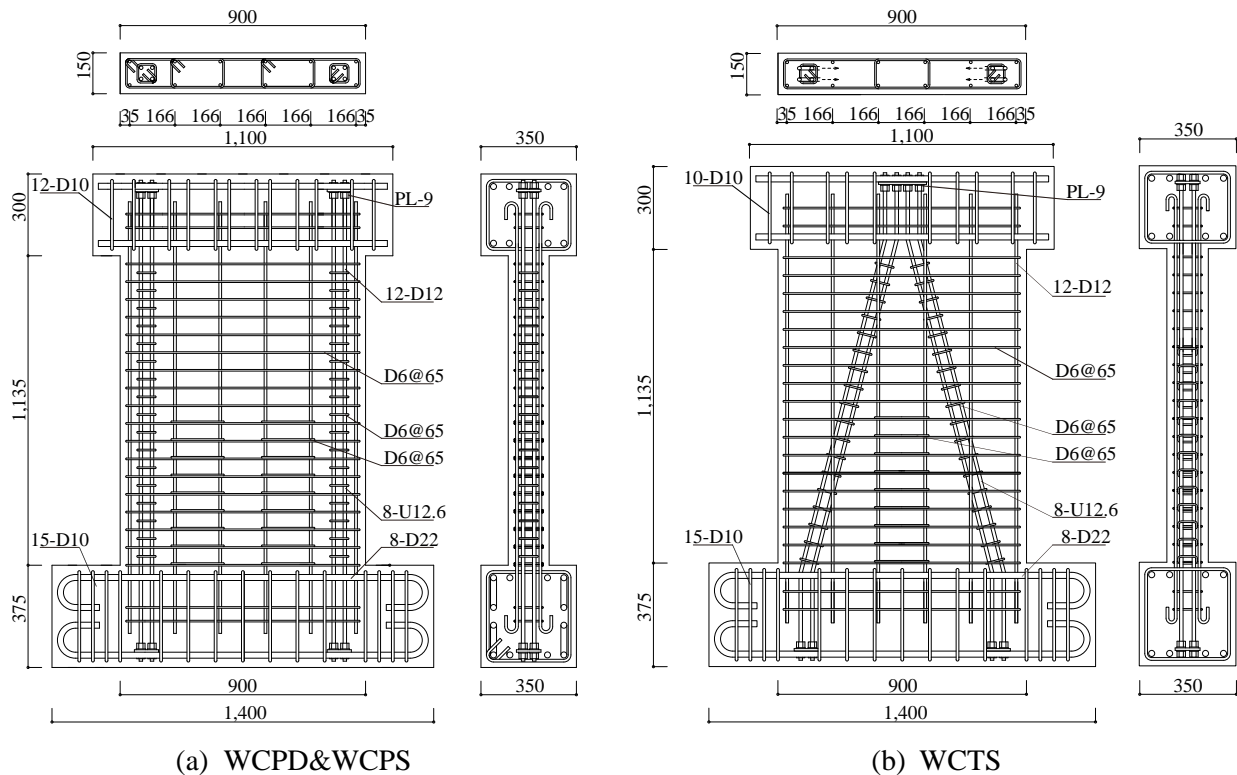(a) WCPD&WCPS   (b) WCTS

Fig. 1 – Dimensions and reinforcement details of test walls

All test walls were 900mm and 150mm in depth and width, respectively. The distance from the action line of the lateral loading to the base of wall was 2025mm to give a shear span ratio of 2.25. As shown in Fig.1, NS D10 rebars with spacing of 166mm and D6 rebars with spacing of 65mm were adopted as the distributed longitudinal and transverse reinforcement in the wall panel of each specimen, respectively, to give a steel ratio of about 0.65%. The primary tensile rebars in the boundary element consisted of four SBPDN rebars of 12.6 mm in diameter with a specific yield strength of 1275MPa and the tensile steel ratio of SBPDN rebars was about 0.37%. In two walls the SBPDN rebars were placed within edge zones parallel to the axis of wall, while in the other the SBPDN rebars were placed in an inverted V-shape within the wall panel. Of three walls, two were tested under reversed cyclic lateral loading and the other was subjected to pseudo-dynamic loading to investigate the effect of the loading rate on the seismic properties of drift-hardening concrete walls.

Table 2 – Mechanical properties of the steels

Notation		Yield strength f_y (MPa)	Yield strain ε_y (×0.01)	Tensile strength f_u (MPa)	Young's modulus E_s (MPa)
D6	SD295A	377	0.20	513	$1.89×10^5$
D10	SD295A	352	0.20	476	$1.74×10^5$
U12.6*	SBPDN 1275/1420	1361	0.84	1470	$2.12×10^5$
*0.2% offset yield strength					

Ready-mixed concrete with a designed compressive strength of 40MPa was used to make the walls. And the actual fc at the stage of testing are listed in Table 1. The axial load ratio applied to each wall was 0.075, which approximately corresponds to gravity load at the base of an eight-story wall.

3

The experimental variables were the loading type (dynamic and static) and the configuration of SBPDN rebars placed in the boundary element (parallel placement and inverted V-shaped placement).

2.2 Details of experiment

2.2.1 Test apparatus and instrumentations

Fig.2 shows the test apparatus used. The lower loading foundation stubs were anchored to the base steel beam, which were also restrained by 8 PC steel bars. Here the base steel beam is a 400-mm-high H-steel beam, which is fixed on the ground. Cyclic lateral loading was applied through a hydraulic actuator of 400kN capacity. This actuator was bolted to the laboratory strong reaction wall at a height of 2025mm from the top surface of foundation stub. A constant axial compressive force was the pre-stress provided through two PC steel bars, and it was measured through a loadcell. During the experiment, the variation range of axial load ratio is from 0.066 to 0.123.
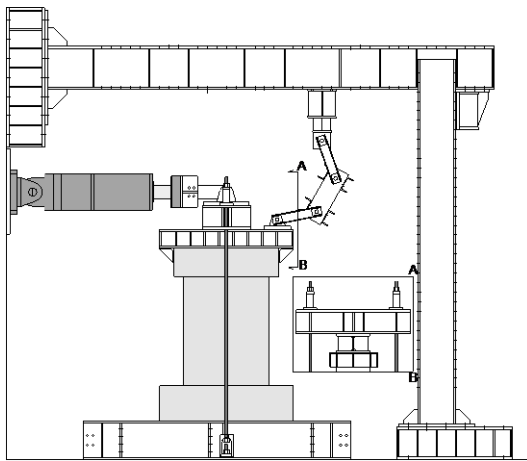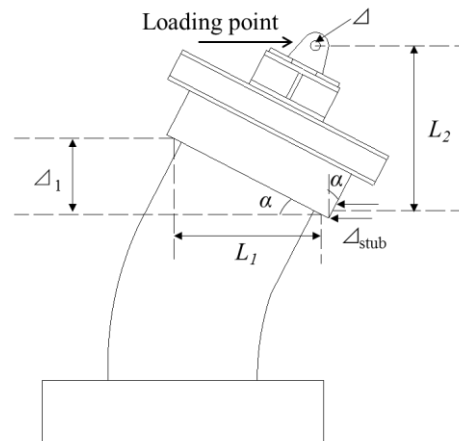

Fig. 2 – Test apparatus

Fig. 3 – Measuring method of drift angle

The drift angle *R* of the wall is calculated by Eq. (1) -(3).

$$\alpha = \frac{\Delta_1}{L_1} \tag{1}$$

$$\Delta = \Delta_{stub} + L_2 \times \alpha \tag{2}$$

$$R = \Delta/h \tag{3}$$

Where α is the rotation of the upper loading stub measured using two displacement transducers, Δ_{stub} is the lateral displacement of the upper loading stub, and L_2 is the vertical distance between the measurement point of Δ_{stub} and the loading point, as shown in Fig. 3, and the part between the loading point and the test wall is assumed as a rigid body.

2.2.2 Particulars of static loading

Specimens WCPS and WCTS were subjected a reversed cyclic lateral loading controlled by the drift angle *R*. Two complete cycles were applied at each level of lateral displacement until drift ratio reached 0.02 rad, and one cycle was applied at each level displacement after drift ratio becomes larger than 0.02rad. The loading program is illustrated in Fig. 4.

2.2.3 Particulars of dynamic loading

Specimen WCPD was subjected to the dynamic loading, which provided the lateral displacement that was the response of a simulation wall under ground motions with multiple speed levels. In this simulation, the test wall
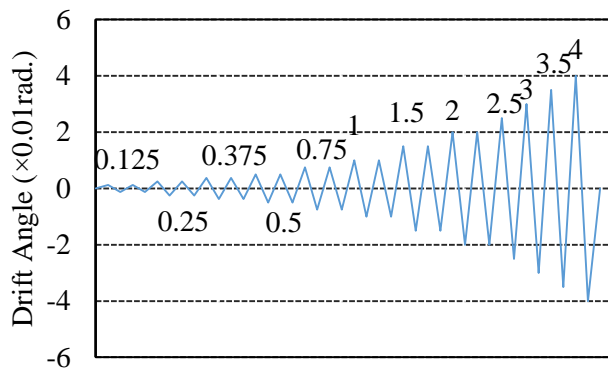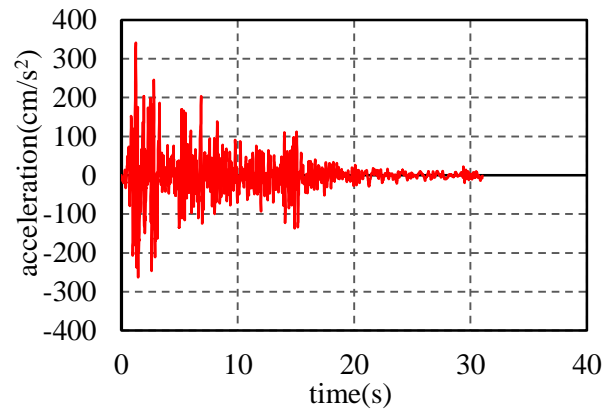
4

Fig. 4 – Loading program

Fig. 5 – El Centro NS time history

Table 3 – Experiment results

WCPS			WCTS			WCPD						
R_{target}	R_{peak}	V_{peak}	R_{target}	R_{peak}	V_{peak}		R_{target}	SF	PGV	Dir.	R_{peak}	V_{peak}
(×10⁻²rad.)	(×10⁻²rad.)	(kN)	(×10⁻²rad.)	(×10⁻²rad.)	(kN)		(×10⁻²rad.)		(cm/s)		(×10⁻²rad.)	(kN)
+0.125	0.101	79.8	+0.125	0.114	81.0	run1	0.125	0.4	13.4	push	0.124	103.5
-0.125	-0.124	-103.2	-0.125	-0.132	-121.9					pull	-0.066	-48.8
+0.25	0.186	113.6	+0.25	0.248	130.0	run2	0.25	0.65	21.8	push	0.219	137.4
-0.25	-0.236	-143.2	-0.25	-0.252	-163.8					pull	-0.125	-110.1
+0.375	0.324	149.7	+0.375	0.373	163.0	run3	0.375	0.9	30.2	push	0.339	169.2
-0.375	-0.351	-173.4	-0.375	-0.380	-192.5					pull	-0.162	-120.4
						run4	/	1	33.5	push	0.403	185.7
										pull	-0.200	-145.0
+0.5	0.444	175.5	+0.5	0.495	188.8	run5	0.5	1.05	35.2	push	0.436	190.9
-0.5	-0.460	-194.7	-0.5	-0.509	-215.1					pull	-0.244	-154.7
+0.75	0.754	250.6	+0.75	0.751	228.2	run6	0.75	1.37	45.9	push	0.662	233.4
-0.75	-0.755	-244.8	-0.75	-0.762	-249.7					pull	-0.598	-233.8
+1.0	1.00	282.8	+1.0	1.01	265.5	run7	1.0(1)	1.53	51.3	push	0.726	240.5
										pull	-0.814	-269.5
-1.0	-1.01	-273.6	-1.0	-0.99	-271.5	run8*	1.0(2)			push	0.862	261.1
										pull	-0.980	-288.0
+1.5	1.50	327.1	+1.5	1.52	306.5	run9	1.5(1)	1.84	61.6	push	0.831	251.2
										pull	-1.17	-308.6
						run10*	1.5(2)			push	0.979	269.9
										pull	-1.30	-311.5
-1.5	-1.50	-320.6	-1.5	-1.49	-302.7	run11**	1.5(3)			push	0.950	259.9
										pull	-1.37	-323.1
						run12**	/	2	67.0	push	1.59	337.6
										pull	-1.59	-342.8
+2.0	2.00	366.3	+2.0	2.28	335.3	run13**	2	2.2	73.7	push	1.57	320.1
-2.0	-2.01	-341.3	-2.0	-1.68	-296.0					pull	-1.87	-356.7

Note: R_{target} is the target drift; R_{peak} is the actual maximum drift; V_{peak} is the force corresponding to R_{peak};
 SF is the scale factor of the ground motion record; PGV is the peak velocity of the ground motion;
 * the target displacement was scaled to 1.2; ** the actuator moved at half real-time speed.

was treated as SDOF system, where the mass was set to 41.3 tons, corresponding to the axial load ratio of 0.075, and the damping ratio was set to 5%. Besides, the spring of the wall model had a trilinear envelope modelled from the measured behavior of specimen WCPS with a hysteresis loop of Takeda model [4]. The fundamental natural period of this system was 0.206 s.

The responses of the simulation wall under ground motions, which is the NS component of the 1940 El Centro Earthquake ground motion, as shown in Fig.5, were analyzed with a time interval of 0.005 s. The time of the ground motion was scaled to $1/\sqrt{2}$ according to the similitude law that was to be applied to the wall of 1/2 scale. The magnitude of the ground motion was adjusted so that the predicted maximum drift of the simulation wall subjected to the ground motion corresponded to the peak drift in each cycle of cyclic lateral loading shown in Fig. 4 till the drift ratio of 0.02 rad., as shown in Table-3. However, when the target peak drift was larger than 0.01 rad., the motion of the actuator could not realize the target displacement with real-time speed. Therefore, for the ground motion targeting the drift of more than 0.01rad., the actuator moved at half real-time speed (where denoted with two asterisks). In some cases denoted with an asterisk in Table 3, the target displacement was simply scaled to 1.2 to compensate the displacement. And the additional cyclic lateral loading was conducted under a quasi-static condition to investigate the seismic behavior of specimen WCPD for the drift ratio of larger than 0.02 rad., as shown in Fig. 4.

3. Experimental results and discussions

3.1 Cracks and damages of specimens

The observation of the cracks and damages on specimens WCPS and WCTS were implemented at the peak of each cycle, while those of specimen WCPD were implemented after each run.

For the damages of wall WCPS and WCTS, the first flexural crack was observed near wall toe at the drift of 0.00125 rad. while shear crack was observed at the drift of 0.0025 rad. Yielding of the longitudinal D10 bars in the wall panel commenced at the drift of 0.0075 rad. The cover concrete began to spall off at the drift of around 0.01 rad and 0.015 rad respectively. For specimen WCPS, buckling of longitudinal D10 bars and yielding of SBPDN bars appeared at the drift of 0.03 rad. The loading of specimen WCPS was terminated after the drift of 0.035 rad., as one of the shear cracks was enlarged too much so that the lateral force and axial force were decreased. For specimen WCTS, the lateral displacement at $R = 0.02$, 0.025 and 0.03 rad. could not be controlled as programed due to errors of the measurement system, resulting in the difference in the envelope lines of the push and pull direction. At the drift of 0.025 rad. the longitudinal D10 bars were buckled and snapped. The loading was terminated during the cycle of 0.04 rad., as tensile rebar of west side buckled so that the lateral force and axial force cannot be maintained.

For the damages of wall WCPD, the first flexural crack was observed near wall toe after deformed at the drift of 0.00403 rad., while shear crack was observed after deformed at the drift of 0.00814 rad. Yielding of the longitudinal D10 bars in the wall panel commenced at the drift of 0.0066 rad. Vertical cracks occurred to the wall toe after the drift of 0.0098 rad., and the cover concrete began to spall off around drift of 0.01170 rad. However, the yielding of tensile rebars did not appear while the target drift of dynamic loading reach 0.02 rad. Therefore, an additional static loading was carried out to reveal the ultimate performance of the specimen. At the drift of 0.02 rad. of static loading, buckling of longitudinal D10 bars appeared. The loading was terminated during the cycle of 0.04 rad. drift, as one of the shear cracks was enlarged too much so that the lateral force and axial force were strongly decreased. Owing to the breaking of the strain gauges at 0.025 rad., yielding of SBPDN bars cannot be recognized.

3.2 Lateral force versus drift ratio relationships of specimens

Fig.6 shows the measured lateral force versus drift ratio relationships of each specimen, whose primary data were listed in Table. 3. For dynamic loading, actual drift did not reach target drift because the speed of actuator cannot correspond to the input waveform accurately.
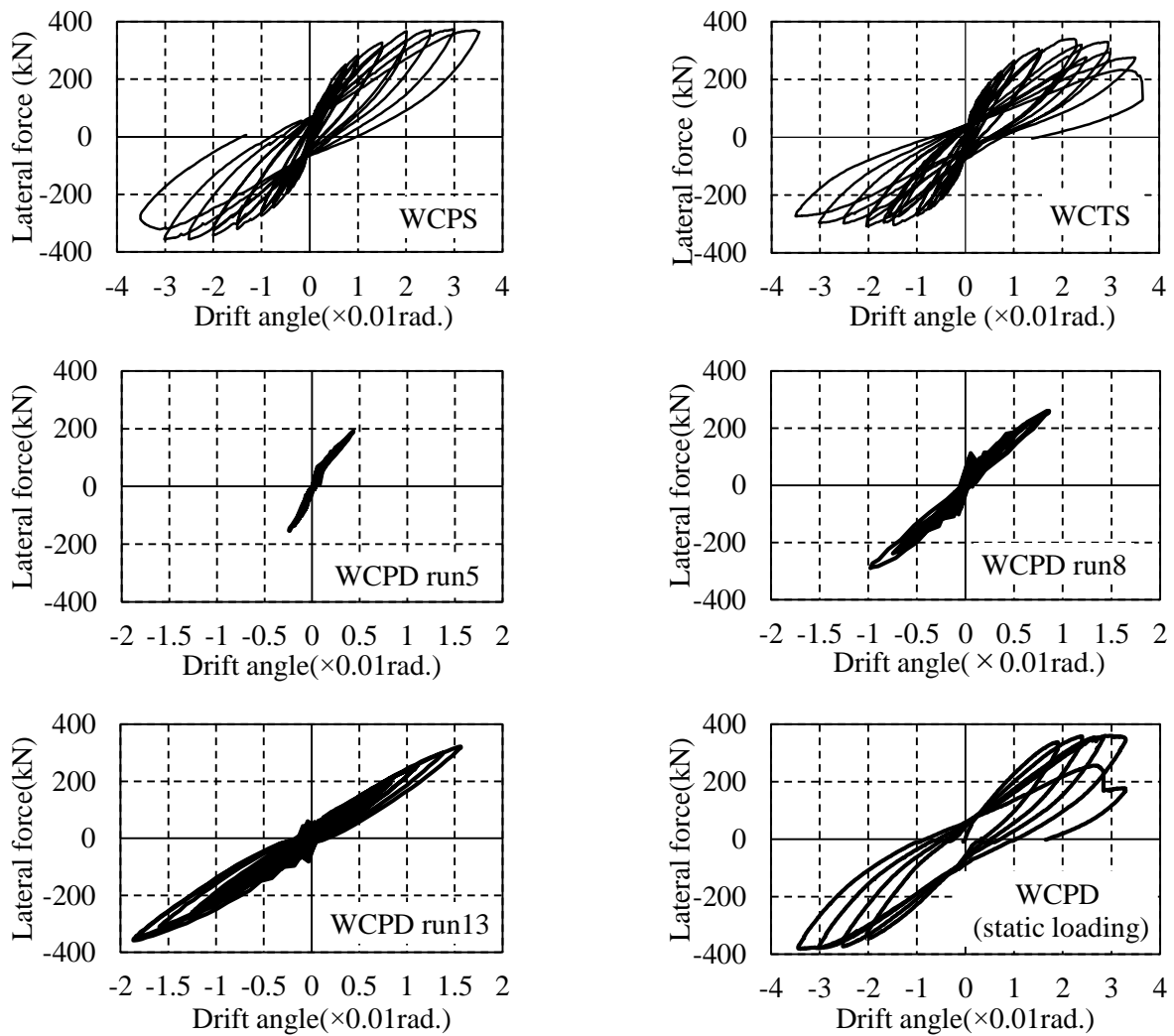
Fig. 6 – Measured lateral load versus drift ratio relationships
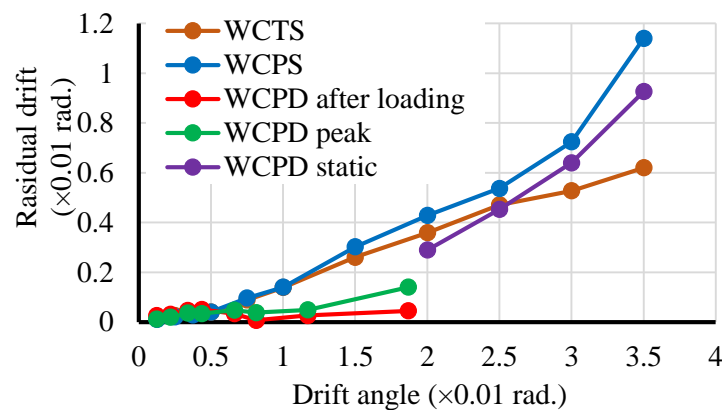

Fig. 7 – Measured residual drift ratio

As can be seen from Fig.6, the lateral resistance of three walls with SBPDN rebars stably increased up to such a large drift level as 0.03 rad., which called typical drift-hardening characteristic. The lateral resistance of walls WCPS and WCPD began to degrade at $R = 0.035$ and 0.04 rad. due to significant shear cracks developing, respectively. On the contrary, the wall WCTS reached an ultimate state at $R = 0.04$ rad. due to

7

buckling of the tensile rebars, instead of shear failure. This indicates that the inverted V-shaped placement of the tensile rebars increased the shear resistance of the wall enough to prevent shear failure of the wall.

The residual drift angle of each experiment wall is as Fig.7 shown. Here the residual drift angle for the specimens subjected to cyclic lateral loading presents the drift angle after unloading in each cycle, while the residual drift for the specimen subjected to dynamic loading was evaluated by two indexes, of which one represents the residual drift after each ground motion and was referred as "final residual deformation", and the other represents the residual drift after unloading from the maximum drift for each ground motion and was referred as "maximum possible residual deformation". In all test walls, the residual drift angles were kept in a very low level as 0.005 rad. after unloading from $R = 0.02$rad., which showed that SBPDN rebars can suppress the residual deformation.

Through the comparison between the results of specimens WCPS and WCTS, it can be investigated that the residual drift angles are almost same before 0.01 rad. The residual drift angle of specimen WCPS exhibited a sharp increase at $R = 0.03$ rad. due to the developement of shear cracks.

By comparing the residual drift ratios of specimens WCPS and WCPD, both the final and the maximum possible residual drift ratios of specimen WCPD were quite smaller than the residul drift ratio of specimen WCPS. On the other hand, for the additional static loading, although the residual drift angle of specimen WCPD is smaller than which of WCPS, the trends of both test walls are same. These results indicates that the seismic behavior of the wall reinforced with SBPDN bars could be affected by the loading program or the loading rate.

3.3 Comparison of the crack widths

Fig. 8 shows the maximum flexural and shear crack widths at peak and unloading timing of each cycle until the peak drift ratio reached 0.02rad. According to Fig. 8-(a) and 8-(b), the trends of drift angle variations for both specimens are similar, so that the influence caused through placement of tensile rebars is indistinct. For specimen WCPS, the crack widths at the peak drift are getting small, while the shear deformation is increasing at the drift of 0.02 rad. Whereas, for specimen WCTS, a similar tread to specimen WCPS didnot appear, and the shear crack widths were quite small in each cycle, compared with WCTS. Therefore, it was found that the shear deviation can be supressed through inverted V-shaped placement of rebars. In addition, through the comparison between Fig. 8-(a) and 8-(c), the residual flexural and shear crack widths of specimen WCPS and specimen WCPD are similar. The result indicates that the residual crack widths of the wall reinforced with SBPDN bars cannot be affected by the loading type.
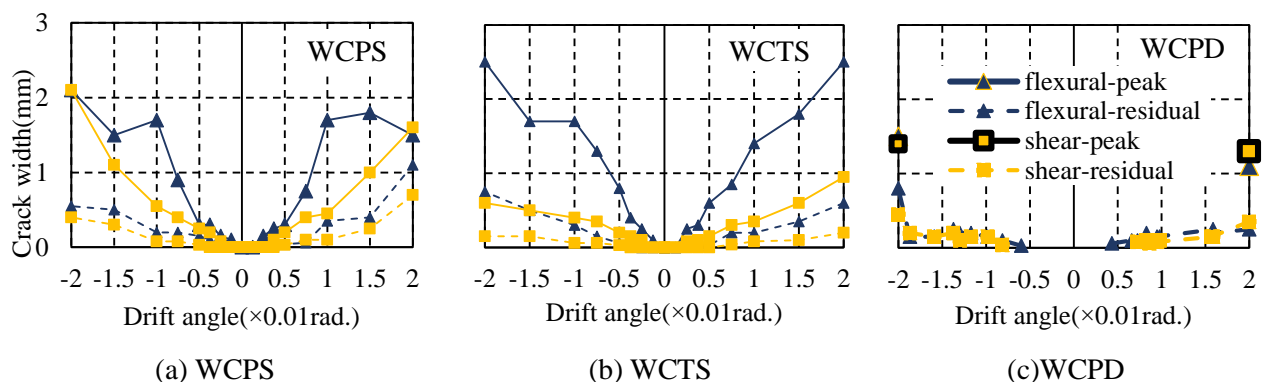

Fig. 8 – Comparison of the crack widths

3.4 Strains of tensile rebars

Fig.9 shows the strain distribution of SBPDN rebars along the wall height. To measure strains in tensile rebars, strain gauges were embedded via an adhesive to the surface of rebars locates 50mm, 145mm, 275mm, 570mm,

8

865mm, 1090mm away from the base of each wall. The red dashed lines represent yield strain of SBPDN rebars. The strains are those measured at several controlling drift ratios. As one can see, for three specimens, the strain gradient along the wall height was very small and that there is not so clear difference among the steel strains on each height after the drift of 0.0075 rad., which is resulted from that bond slippage of SBPDN rebars is low. It can be investigated that, unrelated to loading types, the yielding of SBPDN rebars is delayed through the wider distribution of steel strains, which leads to high drift-hardening effect.
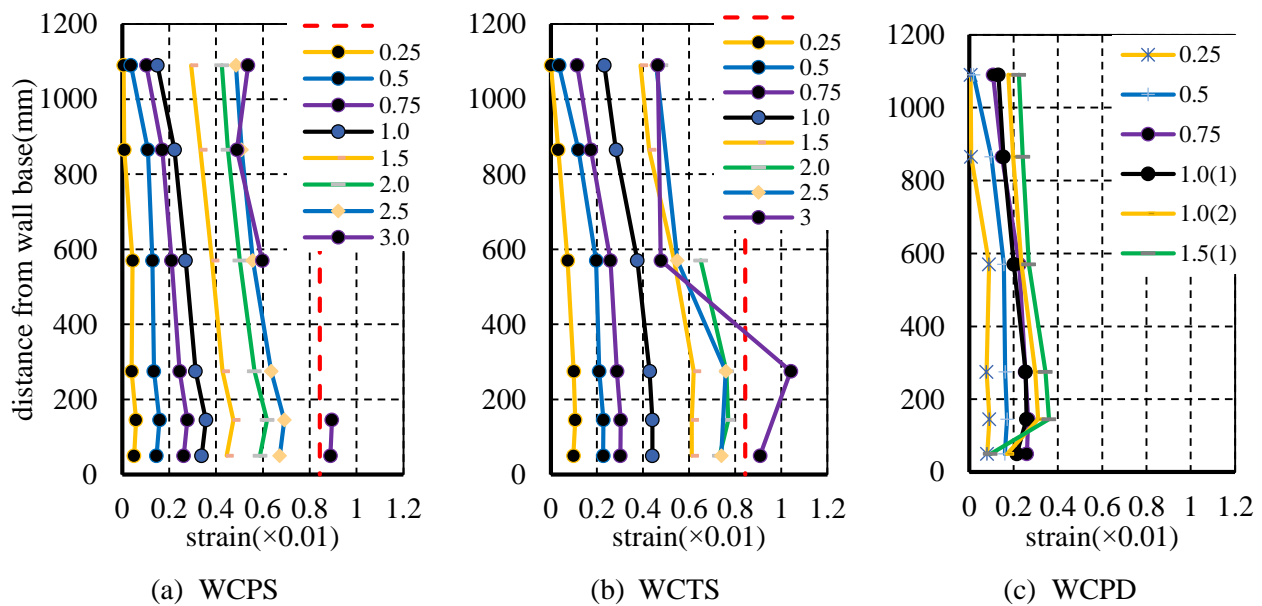

(a) WCPS   (b) WCTS   (c) WCPD

Fig. 9 –Strains distrubution of main reinforcement

4. Evaluation of seismic behavior

4.1 Evaluation of ultimate capacity

Based on previous study [2], it can be known that NewRC block [5] can be used to evaluate the ultimate flexural strength of concrete walls reinforced by SBPDN rebars. In this paper, the comparison between the experimental and calculated results was as Table. 1 shown. The calculated flexural strength agreed very well with the experiment results regardless of the placement of the tensile rebar and the loading condition.

4.2 Analytical method for estimating cyclic performance of test walls

To simulate cyclic behavior of specimens, an analytical method was presented which take account of effect of slippage of the SBPDN rebars [6]. This analysis is based on the following basic assumptions: 1) concrete does not resist tensile stress; 2) the concrete plane remains plane after bending; 3) the constitutive laws of the concrete are known from Reference [5]; 4) the bond-slip relationship of the SBPDN rebar follows the model developed by Reference [7]; 5) the lateral displacement of column concentrate in the plastic hinge region of 0.9D (where D is the section diameter of the wall); 6) strain and stress of the SBPDN rebar are uniformly distributed within the plastic hinge region.

The comparisons of the calculated and experimental results were shown in Fig.10. The hysteresis properties of analyzed and experimental results for specimen WCPS can match ideally until the drift angle of 0.035 rad., while for specimen WCTS, the results can match well until the spalling off of the concrete began at drift angle of 0.025 rad. Therefore, it can be concluded that with the consideration of bond slippage, the hysteresis properties could be simulated accurately. Whereas, for specimen WCPD, the lateral resistance of peak drift could be predicted accurately by this analysis. However, for the unloading behavior, the results are

9

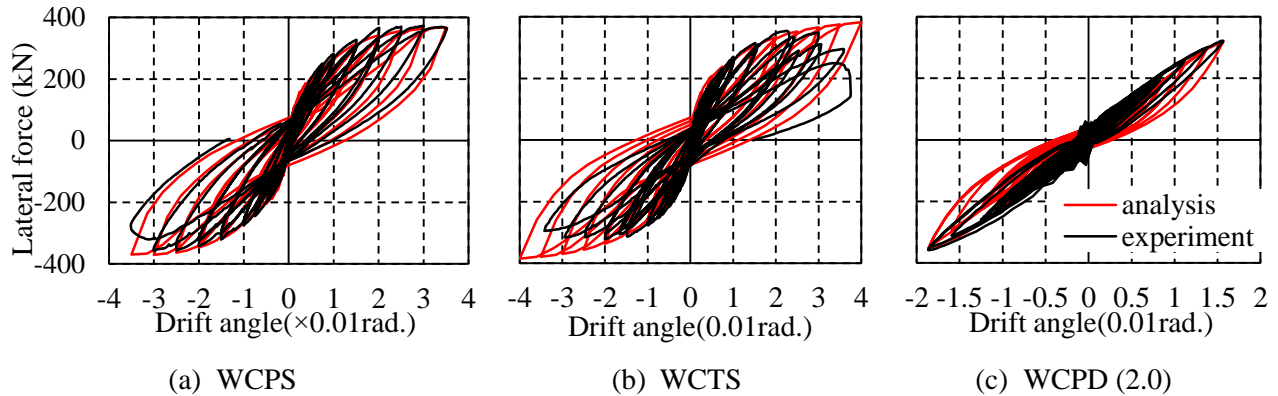described as a plump hysteresis loop, due to the loading speed.

Fig. 10 –Comparison of analysis and experiment

5. Conclusion

To verify seismic behavior of the concrete walls reinforced by SBPDN rebars, three rectangular concrete walls were fabricated and tested under pseudo-dynamic loading and/or statically cyclic loading while subjected to a constant compression. Based on the experimental and analytical results described in this paper, the conclusions can be described as following:

1) The lateral resistance of three test walls with SBPDN rebars stably increased up to such a large drift level as 0.03 rad., which showed typical drift-hardening characteristic. In all test walls, the residual drift angles were kept under a very low level as 0.005 rad. before drift angle reach 0.02rad., which showed that SBPDN rebars can suppress the residual deformation.

2) Rectangular concrete walls reinforced by SBPDN bars could provide the same lateral force during dynamic loading as which during static loading.

3) The test wall with inverted V-shaped placement of rebars could suppress shear failure, and held higher deformation performance than test wall with parallel placement of rebars.

4) The cyclic behavior of the proposed drift-hardening concrete walls was evaluated by the analytical method that can take account of effect of slippage of the SBPDN rebars. A quite satisfactory agreement was observed between the experimental hysteresis loops and the calculated results, which implies the reliability and accuracy of the analytical method.

6. Acknowledgements

7. References

[1] AIJ Standard for Structural Calculation of Reinforced Concrete Structures, 2010

[2] Fujitani T., Sun Y., Takeuchi T., Wei C. (2018): Study on effect of strength of rebars on the seismic performance of rectangular concrete walls, *Proceedings of the Japan Concrete Institute*, **40** (2), 313-318, (in Japanese)

[3] Wei C., Sun Y., Takeuchi T., Fujitani T. (2018): Study on seismic behavior of concrete walls with triangular reinforcement, *Proceedings of the Japan Concrete Institute*, **40** (2), 319-324, (in Japanese)

[4] Takeda T. (1970): Reinforced Concrete Response to Simulated Earthquakes. *Journal of the Structural Division*, ASCE 96(ST12), 2557-2573,

[5] Sun Y., Sakino K., Yoshioka T. (1996): Flexural behavior of high-strength RC columns confined by rectilinear reinforcement, *Journal of Structural and Construction Engineering*, Architectural Institute of Japan, **486**, 95-106.

[6] Sargayan G, Cai G, Takeuchi T, Sun Y (2017): Seismic behavior and assessment of drift-hardening concrete columns, *16th World Conference on Earthquake Engineering*, Santiago, Chile

[7] Funato Y., Sun Y., Takeuchi T., Cai G. (2012): Modeling and application of bond characteristic of high-strength reinforcing bar with spiral grooves, *Proceedings of the Japan Concrete Institute,* **34**(2), 157-162, (in Japanese).